DOI 10.5162/IMCS2012/4.3.4

Synthesis and gas sensing properties of hierarchical SnO_2 nanostructures

Peng Sun, Fasheng Yang, Houbo Zhang, Yanfeng Sun, Geyu Lu**
State Key Laboratory on Integrated Optoelectronics, College of Electronic Science and Engineering, Jilin University, 2699 Qianjin Street, Changchun 130012, China,
syf@jlu.edu.cn, lugy@jlu.edu.cn

Abstract:
We have successfully prepared hierarchical SnO_2 nanostructures via a facile hydrothermal synthesis method. Field emission scanning electron microscopic and transmission electron microscopic results reveal that these hierarchical nanostructures are built from two-dimensional (2 D) nanosheets with edge thicknesses of about 8 nm. Gas sensing tests show that the sensor using hierarchical SnO_2 nanosheets exhibits high response and good selectivity to ethanol. Moreover, the sensor shows superior gas sensing performance compared with the sensor based on conventionally prepared SnO_2 nanoparticles. For example, at an ethanol concentration of 100 ppm, the response of the SnO_2 nanosheets is about 32.7, while the response is about 11 for nanoparticles. The enhancement in gas sensing properties is attributed to their unique structures.

Key words: hydrothermal synthesis, SnO_2, hierarchical nanostructures, and gas sensor

Introduction

As an n-type wide-band gap (E_g=3.6 eV) semiconductor, SnO_2 is one of most intensively studied materials due to its widely important applications such as gas sensors and solar cells [1, 2]. To date, various techniques have been employed to synthesize SnO_2 nanostructures with diverse morphologies [3-6].

It is well known that the most important aspect of investigation of chemical sensors based on semiconductor oxide is its sensitivity, selectivity, and stability. Up to now, great efforts have been made to better resolve these problems. The synthesis of sensing materials with novel structure is one of the most promising solutions because they can be achieved easily. Yamazoe demonstrates that a reduction in materials size can significantly enhance sensor performance [7]. However, the aggregation between the nanoparticles becomes very strong because the Van der Waals attraction is inversely proportional to the particle size. Under this contiguration, a high sensitivity can't be achieved because the change in resistance occur only the surface region. In this respect, hierarchical structures composed of nanosized building blocks have attracted considerable attention due to their low density, large surface area, and surface permeability.

In our work, three-dimensional (3 D) SnO_2 hierarchical architectures were synthesized by a simple hydrothermal method. A comparative gas sensing properties investigation between as-synthesized flower-like SnO_2 nanosheets and SnO_2 nanoparticles was performed to demonstrate the good gas sensing properties of the 3 D nanostructures.

Experimental

All the reagents in the experiment were purchased from Beijing Chemical Reagent and used as received without further purification. Typically, $SnSO_4$ (0.1 g), $Na_3C_6H_5O_7 \cdot 2H_2O$ (1.37 g), were dissolved in a glycerol-water solution with vigorous stirring. Then 0.3 mL HCl solution was added in the above mixture. The reaction mixture was transferred into a Teflon-lined stainless-steel autoclave, kept at 180 °C for 24 h. Finally, the precipitates were collected by centrifugation, washed several times with distilled water and absolute ethanol, respectively, and dried in air at 80 °C.

The X-ray diffraction (XRD) pattern was recorded with a Rigaku D/max-2500 diffractometer with Cu Kα radiation (λ=1.5418 Å) in the range of 20-80°. Filed-emission scanning electron microscopy (FESEM) observations were carried out with a JEOL JSM-7500F microscope, operated at an acceleration voltage of 15 kV. Transmission electron microscopy (TEM), selected-area electron diffraction (SAED), and high-resolution

transmission electron microscopy (HRTEM) measurements were obtained on a JEOL JEM-2100 microscope operated at 200 kV.

Results and discussion

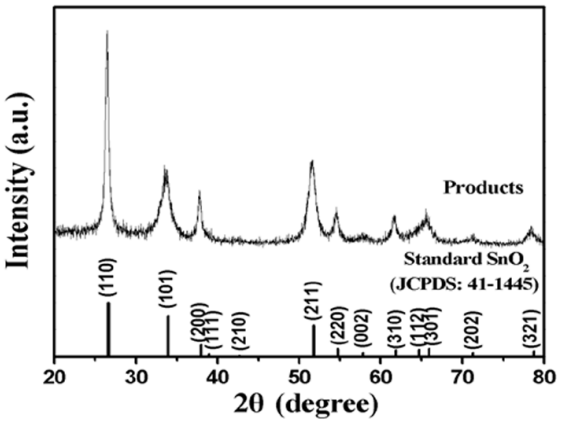

Fig. 1. XRD pattern of the as-synthesized product.

The typical XRD pattern of the product is shown in Fig. 1, from which all of the diffraction peaks could be well indexed to tetragonal SnO_2 (JCPDS card no. 41-1445). No diffraction peaks from any other impurities were observed, indicating the high purity of the products. Compared with those of the bulk material, the peaks were relatively broadened, which demonstrated that the SnO_2 had a small crystal size. The mean crystallite size was calculated to be around 10 nm, which was correspond to the thickness of nanosheets, using the Debye-Scherer formula, $D = 0.89\lambda/(\beta\cos\theta)$, where λ is the X-ray wavelength, θ is the Bragg diffraction angle and β is the peak width at half maximum.

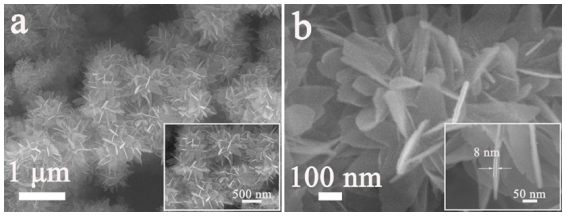

Fig. 2. (a) A panoramic; (b) enlarged FESEM images of the product. The insets show high-magnification FESEM images.

The morphologies and microstructures of the as-prepared products were illuminated by FESEM observations. A panoramic FESEM image of as-sintered products is shown in Fig. 2a, from which flower-like nanostructures were clearly observed. No other morphologies could be detected, indicating a high yield of these 3 D nanostructures. It can be seen that the SnO_2 products had a uniform size of about 500 nm (the inset of Fig. 2a). The enlarged FESEM image of an individual SnO_2 with a hierarchical architecture, as shown in Fig. 2b, indicates that the flower-like nanostructures were constructed by many 2 D nanosheets. The high-magnification FESEM image (the inset of Fig. 2b) shows the detailed morphological information of the nanosheets. It can be observed that the edge thickness of nanosheets was about 8 nm.

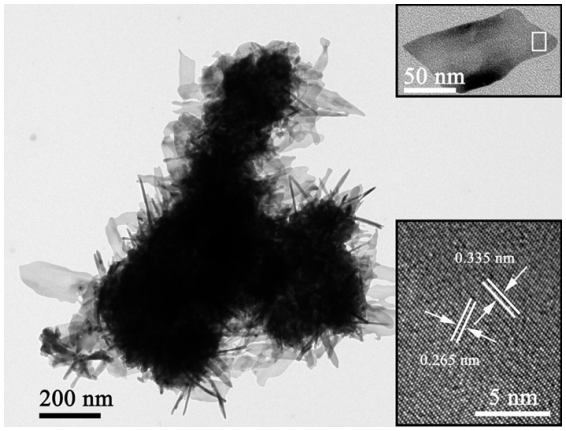

Fig. 3. The typical TEM image of the as-prepared flower-like SnO_2 nanostructures. The insets show high-magnification TEM image of an individual nanosheet and HRTEM image.

More detailed structural analysis of the present nanostructures was carried out using TEM and HRTEM. From the low-magnification TEM images in Fig. 3, it is apparent that the shape of product was similar to those of the SEM observations. The inset in Fig. 3 shows the HRTEM image obtained from the marked fringe of the nanosheet in upper inset, from which the lattice fringes could be observed clearly and the lattice spacing was 0.335 and 0.265 nm, corresponding to the (110) and (101) planes of SnO_2. The result confirms the single-crystal structure of nanosheets.

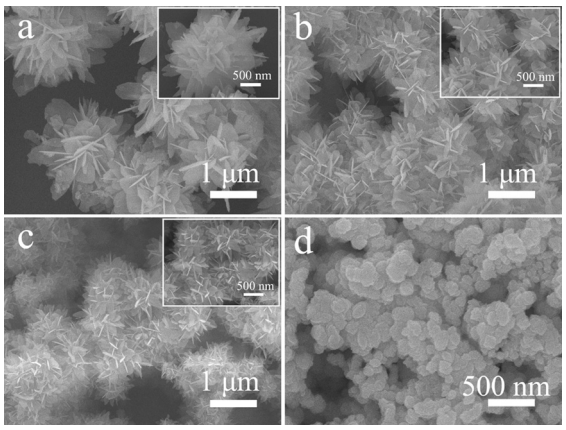

Fig. 4. FESEM images of product obtained with different HCl content: (a) 0.0, (b) 0.1, (c) 0.3, and (d) 0.9 mL. The insets of a, b and c show the enlarged image

The influence of experimental parameter on the microstructures of final as-prepared products was investigated systemically. The result shows

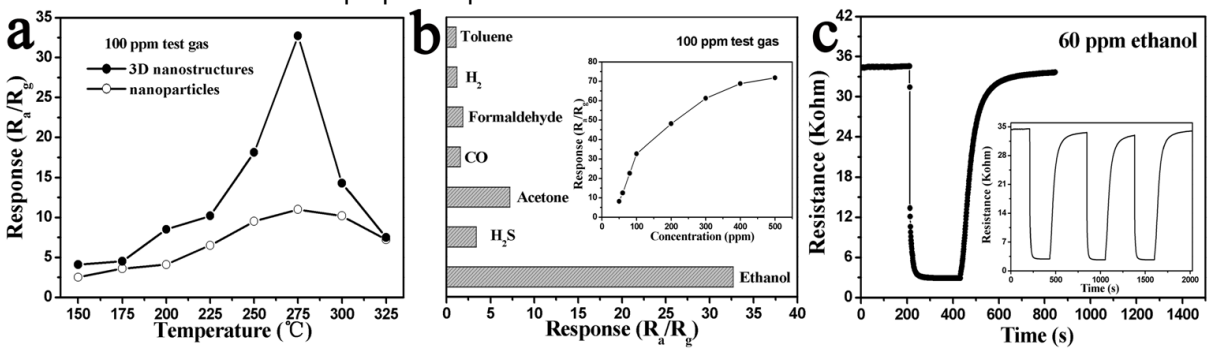

Fig. 4. (a) Sensors response as a function of operating temperatures; (b) Response of sensor to 100 ppm various testing gases. The inset shows response versus ethanol concentration. (c) Response transients of the sensor to 60 ppm ethanol. The inset displays three periods of response curve.

that the amounts of HCl played an important role in controlling the size of the SnO_2 microcrystals. Keeping other conditions unchanged, in the absence of HCl, the resultant products consisted of flower-like nanostructures with a size of about 2 μm, as shown in Fig. 4a. The inset shows that the thickness of nanosheets was about 20-30 nm. With the introduction of HCl (0.1 ml) into the solution, the flower-like nanostructures were maintained. However, the size of product was reduced, from primary 2 μm became current 1μm (Fig. 4b). The thickness was decreased to 10-15 nm, as shown in the inset of Fig. 4b. As the amount of HMT was increased to 0.3 ml, the morphology of product remained unchanged, the thickness was further reduced (Fig. 4c and the inset), the detailed structure characteristics of them have been described previously. Further increase of HCl (0.9 ml), the FESEM image indicates that these flower-like nanostructures transformed into the agglomerates with the size of about 100-200 nm, as shown in Fig. 4d. Therefore, on the basis of the morphological study, it can be concluded that HCl plays an important role in forming flower-like SnO_2 nanostructures and controlling their size.

Gas sensors show important applications in our daily life and industry. For comparison, two gas sensors were fabricated from the as-synthesized flower-like SnO_2 hierarchical nanosheets and SnO_2 nanoparticles synthesized conventionally. It is well known that the response of a gas sensor is highly influenced by its operating temperature [8, 9]. In order to determine the optimum operating temperature, the response of sensors based on as-prepared hierarchical SnO_2 nanostructures and nanoparticles to 100 ppm ethanol was investigated as function of operating temperature, as shown in Fig. 5a. Obviously, the response of each sensor was strongly dependent on the operating temperature. Two sensors had the same of optimal operating temperature (275 °C), at which the sensor exhibited the highest response to ethanol gas. At various temperatures, the sensor based on flower-like SnO_2 hierarchical nanosheets exhibited higher response to ethanol gas compared with that of sensor using nanoparticles. The result suggests that the as-synthesized 3 D hierarchical SnO_2 architectures had better gas sensing property and was a promising candidate for high performance ethanol sensor.

Selectivity is an important parameter of a gas sensor. Fig. 5b shows a bar graph of the responses of the sensor based on as-prepared flower-like SnO_2 nanosheets to a variety of gases, such as ethanol, acetone, CO, etc. All of the gases were tested at an operating temperature of 275 □ with a concentration of 100 ppm. The results indicate that the sensor exhibited the highest response to ethanol among the tested gas and the response was about 32.7. The response towards toluene was no greater than 2. Therefore, it was concluded that the sensor using as-synthesized hierarchical SnO_2 nanosheets showed selectivity toward ethanol as oppose to any other gas. The relationship between response and ethanol concentrations for the sensor at operating temperatures of 275 □ is displayed in the inset of Fig. 5b. From the curve, it is found that the responses of sensor increased with the gas concentrations. Moreover, the responses were proportional to the increasing concentrations of ethanol, when the gas concentrations were correspondingly low. Above 400 ppm, the responses increased slowly with the gas concentrations, which indicated that the sensor tended to saturation gradually.

For a gas sensor, the response and recovery times are also important parameters. Rapid

response and recovery to a target gas are demanded for practical application. Fig. 5c shows the response transients of sensor to 60 ppm ethanol at 275 □. The result indicates that the sensor immediately responded when ethanol was introduced. The response and recovery times of the sensor using as-prepared hierarchical SnO_2 nanosheets were 11 and 125 s, respectively. The three reversible cycles of the response curve indicated a stable and repeatable characteristic, as shown in the inset of Fig. 5c.

The sensing mechanism of metal oxides gas sensors has been clarified in previous works. The most widely accepted model is based on the change in resistance of the sensor upon exposure to different gas atmospheres. When the sensor based on as-prepared hierarchical SnO_2 nanosheets is exposed to air, oxygen molecules adsorb onto the surfaces of nanosheets, and form chemisorbed oxygen species by capturing electrons from the conductance band of SnO_2. The decrease of the electron concentration in the conduction band leads to stabilization of high surface resistance. When the sensor is exposed to ethanol, CO, or other reductive gas atmospheres at a moderate temperature, these gas molecules will react with the adsorbed oxygen species on its surfaces. This process releases the trapped electrons back to the conductance band of SnO_2 and results in an increase the electron concentration. This effect eventually increases the conductivity of the SnO_2 nanosheets. The high response of the sensor to ethanol is attributed to their unique architectures. These structures were randomly oriented to provide a large number of pores and a higher surface area than that of other types of sensors. This network of pores enables gas to diffuse easily toward all of the surfaces of SnO_2 nanosheets. Therefore, the sensor is expected to be high response to ethanol.

Conclusions

In summary, a simple one-step solution route was reported for the formation of 3 D SnO_2 nanostructure with hierarchical flower-like shapes, which were composed of many 2 D nanosheets with the thickness of about 8 nm. The amount of HCl exerted crucial influences on the final size and morphology. Moreover, gas-sensing properties of our SnO_2-based sensor exhibited high response to ethanol. The enhanced gas sensing performances were attributed to the unique hierarchical structure, which can significantly facilitate gas diffusion and mass transportation in sensing materials.

Acknowledgements

This work was supported by NSFC (No. 61074172, 61134010, 61006055) and Program for Changjing Scholars and Innovative Research Team in University (No. IRT1017) and Jilin province science and technology development plan program (20106002).

References

[1] A. Kolmakov, Y. Zhang, G. Cheng, M. Moskovits, Detection of CO and O_2 using tin oxide nanowire sensors, *Adv. Mater*. 15, 997-1000 (2003); doi: 10.1002/adma.200304889

[2] A. Kay, M. Grätzel, Dye-Sensitized Core-Shell Nanocrystals: Improved Efficiency of Mesoporous Tin Oxide Electrodes Coated with a Thin Layer of an Insulating Oxide, *Chem. Mater.* 14, 2930-2935 (2002); doi: 10.1021/cm0115968

[3] Y. Liu, J. Dong, M. Liu, Well-aligned “nano-box-beams” of SnO_2, *Adv. Mater*. 16, 353-356 (2004); doi: 10.1002/adma.200306104

[4] Z.R. Dai, Z.W. Pan, Z.L. Wang, Growth and Structure Evolution of Novel Tin Oxide Diskettes, *J. Am. Chem. Soc*. 124, 8673-8680 (2002); doi: 10.1021/ja026262d

[5] Y. Lilach, J.P. Zhang, M. Moskovits, A. Kolmakov, Encoding Morphology in Oxide Nanostructures during Their Growth, *Nano Lett*. 5, 2019-2022 (2005); doi: 10.1021/nl051543f

[6] D.F. Zhang, L.D. Sun, J.L. Yin, C.H. Yan, Low-temperature fabrication of highly crystalline SnO_2 nanorods, *Adv. Mater*. 15, 1022-1025 (2003); doi: 10.1002/adma.200304899

[7] N. Yamazone, New approaches for improving semiconductor gas sensors, *Sens. Actuators. B* 5, 7-19 (1991); doi: 10.1016/0925-4005(91)80213-4

[8] V.R. Shinde, T.P. Gujar, C.D. Lokhande, Enhanced response of porous ZnO nanobeads towards LPG: Effect of Pd sensitization, *Sens. Actuators B* 123, 701-706 (2007); doi: 10.1021/j.snb.2006.10.003

[9] H. Gong, J.Q. Hu, J.H. Wang, C.H. Ong, F.R. Zhu, Nano-crystalline Cu-doped ZnO thin film gas sensor for CO, *Sens. Actuators B* 115, 247-251 (2006); doi: 10.1021/j.snb.2005.09.008

[10] Z. Gergintschew, H. Förster, J. Kositza, D. Schipanski, Two-dimensional numerical simulation of semiconductor gas sensor, *Sens. Actuators B* 1, 170-173 (1995); doi: 10.1016/0925-4005(94)01580-B

[11] D.E. Williams, Semiconductor oxides as gas-sensitive resistors, *Sens. Actuators B* 57, 1-16 (1999); doi: 10.1016/S0925-4005(99)00133-1

[12] H. Gong, Y.J. Wang, S.C.Teo, L. Huang, Interaction between thin-film tin oxide gas sensor and five organic vapors, *Sens. Actuators B* 54, 232-235 (1999); doi: 10.1016/S0925-4005(99)00083-0